Thin-Layer Fe_2TiO_5 on Hematite for Efficient Solar Water Oxidation

Jiujun Deng,[†] Xiaoxin Lv,[†] Jinyin Liu,[†] Hui Zhang,[†] Kaiqi Nie,[†] Caihao Hong,[‡] Jiaou Wang,[‡] Xuhui Sun,[*,†] Jun Zhong,[*,†] and Shuit-Tong Lee[†]

[†]Soochow University-Western University Centre for Synchrotron Radiation Research, Institute of Functional Nano and Soft Materials Laboratory (FUNSOM) and Collaborative Innovation Center of Suzhou Nano Science & Technology, Soochow University, Suzhou 215123, China and [‡]Beijing Synchrotron Radiation Facility, Institute of High Energy Physics, Beijing 100049, China

ABSTRACT A thin Fe_2TiO_5 layer was produced on hematite either by evaporating a $TiCl_4$ solution on FeOOH or by a simple HF-assisted Ti treatment of FeOOH, both followed by annealing. The prepared Fe_2TiO_5-hematite heterostructure showed a significant enhancement in photocurrent density compared to that of the pristine hematite. For example, the sample after HF-assisted Ti treatment exhibited a significantly enhanced photocurrent of 2.0 mA/cm^2 at 1.23 V *vs* RHE. Moreover, the performance of the Fe_2TiO_5-hematite heterostructure can be further improved by coupling with Co-Pi catalysts, achieving a higher photocurrent of 2.6 mA/cm^2 at 1.23 V *vs* RHE. Synchrotron-based soft X-ray absorption spectroscopy analyses clearly revealed the existence of an Fe_2TiO_5 structure on hematite forming a heterojunction, which reduced the photogenerated hole accumulation and then improved the performance.

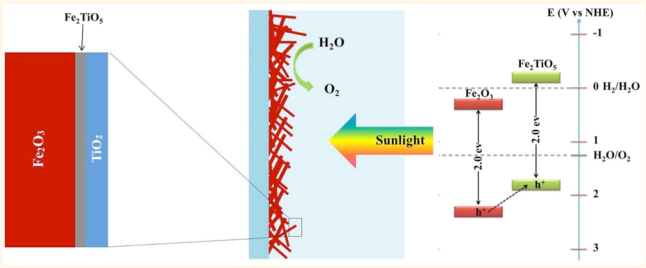

KEYWORDS: Ti treatment · hematite nanostructures · solar water oxidation

Hematite is a good photocatalyst for solar water oxidation because of its favorable optical band gap (2.1–2.2 eV), low cost, abundance, and chemical stability in an oxidative environment.[1−5] However, its practical performance for solar water oxidation is still poor due to various factors such as improper band edge position, low conductivity, poor oxygen evolution reaction kinetics, and short hole diffusion length (2–4 nm).[6−8]

Many efforts have been taken to improve the performance of hematite photoelectrodes.[1−21] Among them a benchmark performance with a photocurrent value of 3.3 mA/cm^2 at 1.23 V *vs* a reversible hydrogen electrode (RHE) and a plateau photocurrent of 3.75 mA/cm^2 was achieved by the cauliflower-type hematite nanostructure prepared by atmospheric pressure chemical vapor deposition (APCVD) with an IrO_2 catalyst.[5] However, the IrO_2/hematite photoanodes showed instability on short time scales, and an effective cobalt phosphate (Co-Pi) catalyst was developed to overcome this problem with a decreased photocurrent of 2.8 mA/cm^2 at 1.23 V *vs* RHE. Recently many other methods such as the hydrothermal method,[21] colloidal nanocrystal deposition,[19] and ultrathin films of hematite on a 3D nanophotonic structure were developed to prepare highly efficient hematite photoanodes with photocurrents of 2.7–3.05 mA/cm^2 at 1.23 V *vs* RHE.[19−21] Ti-based treatments have also been widely used and shown to be very effective methods to improve the performance of hematite photoanodes.[12−19] Ti-based coating on hematite was shown to effectively enhance the performance with an obvious cathodic shift of the onset potential and increased photocurrent.[15] Ti-doping in hematite *via* various approaches such as atomic layer deposition (ALD),[13] the deposition–annealing process,[17] or sol-flame synthesis,[18] has also been widely used to improve the performance of hematite with increased photocurrent and reduced onset potential.[12] Numerous mechanisms have been proposed to explain the effect of Ti-based treatments. Among them Ti substitution of Fe in hematite (the formation of $FeTiO_3$ with Fe^{2+}) with improved donor density has been widely reported.[6,12,17] However, Zandi *et al.* showed that the

* Address correspondence to jzhong@suda.edu.cn (J. Zhong); xhsun@suda.edu.cn (X. Sun).

Received for review February 13, 2015 and accepted April 17, 2015.

Published online April 17, 2015
10.1021/acsnano.5b01028

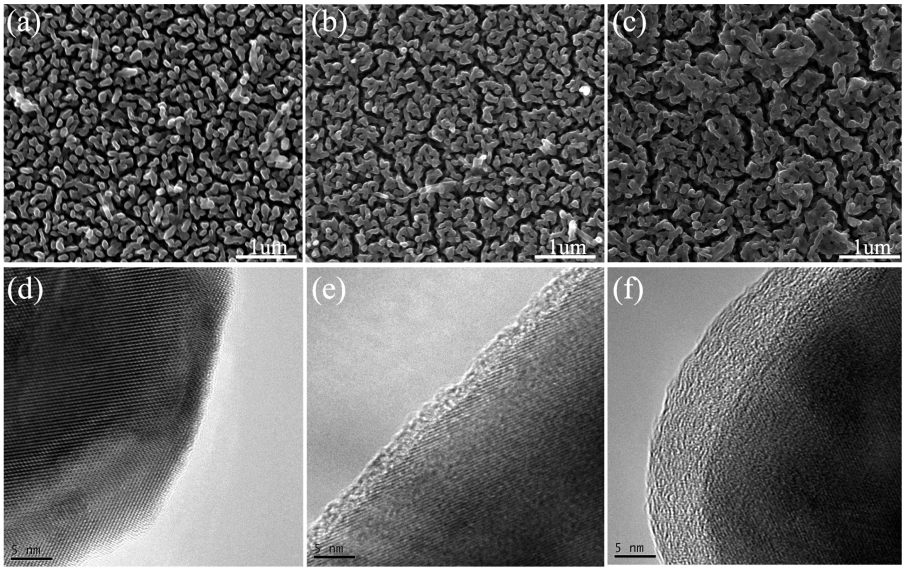

Figure 1. (a−c) SEM images of the Ti-treated hematite nanostructures with different treatment time: 0 s (pristine), 2, and 20 s, respectively. (d−f) HRTEM images of the corresponding samples in a−c.

improved photoactivity of Ti incorporation in hematite could not be simply attributed to the enhanced conductivity.[13] Meanwhile no Fe^{2+} signal could be found in various Ti-treated hematite nanostructures.[12] Understanding the detailed mechanism of Ti-based treatment is still an open question.[12,13]

Here we report the preparation of a new Fe_2TiO_5-hematite heterostructure for solar water oxidation either by evaporating a $TiCl_4$ solution on FeOOH or by a HF-assisted Ti treatment of FeOOH, both followed by annealing. The Fe_2TiO_5-hematite heterostructure shows significantly improved performance compared to that of the pristine hematite. Especially, the HF-assisted Ti treatment results in an ultrathin Fe_2TiO_5 layer on hematite, leading to a high photocurrent (2.0 mA cm^{-2} at 1.23 V *vs* RHE) that is 3 times higher than that of the pristine hematite for solar water oxidation. Moreover, the Fe_2TiO_5-hematite heterostructure can be well coupled with Co-Pi catalysts to yield a higher photocurrent of 2.6 mA/cm^2 at 1.23 V *vs* RHE and a max photocurrent of 3.62 mA/cm^2 at 1.6 V *vs* RHE. The results are comparable to the high performance reported recently,[19−21] especially considering our facile method of HF-assisted Ti treatment only by immersing FeOOH in Ti-dissolved HF solution. The formation of Fe_2TiO_5 is clearly identified by using soft X-ray absorption spectroscopy (XAS), which forms a heterojunction with hematite, reducing photogenerated hole accumulation to improve the performance. The facile synthesis of the new heterojunction structure stands for an effective method to improve the performance of hematite for solar water oxidation. Moreover, the formation of an Fe_2TiO_5-hematite heterostructure can be used to understand the enhanced performance of other Ti treatment processes in hematite.

RESULTS AND DISCUSSION

Two different Ti treatments of hematite were used in this work, while the FeOOH on FTO substrate was prepared by a hydrothermal method.[11] One type of Ti treatment was to evaporate a $TiCl_4$ solution on the surface of FeOOH with subsequent annealing (labeled as Ti-treated hematite; see the Supporting Information S1). The other way was a HF-assisted Ti treatment by immersing the FeOOH into a Ti-dissolved HF solution with subsequent annealing (labeled as HF-Ti-treated hematite; see the Supporting Information S2). The Ti-treated hematite samples by $TiCl_4$ will be first discussed. $TiCl_4$ is a highly volatile metal halide, which forms an opaque cloud of amorphous titanium dioxide (TiO_2) and hydrogen chloride (HCl) when exposed to humid air. A detailed description of the preparation process is shown in the Experimental Section. Scanning electron microscopy (SEM) images of the pristine and Ti-treated hematite nanostructures are shown in the top panels of Figure 1. The pristine hematite (0 s) is a thin film of vertical nanorods on the fluorine-doped tin oxide (FTO) substrate similar to that in the literature.[22,23] The Ti-treated sample with a short treating time (2 s) in Figure 1b has a similar morphology to that of the pristine hematite. However, a longer treating time of 20 s obviously results in a coating layer on hematite in Figure 1c. High-resolution transmission electron microscopy (HRTEM) images of the corresponding samples are shown in the bottom panels of Figure 1. The pristine hematite shows a clear crystal structure of hematite with little or no surface coating. However, an obvious surface coating layer of about 2 and 7 nm on Ti-treated samples can be observed in Figure 1e and f, respectively. The coating layers show an amorphous structure and are expected to

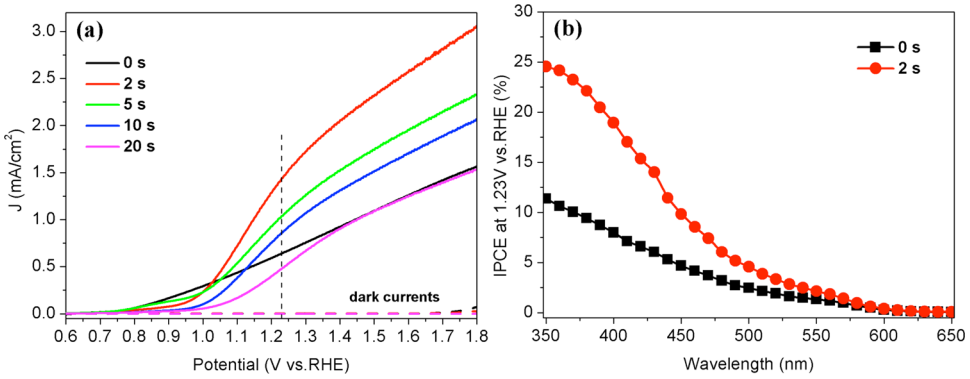

Figure 2. (a) *J*−*V* curves of the pristine (0 s) and Ti-treated hematite photoanodes with different treatment times (2, 5, 10, and 20 s). (b) IPCE spectra of the pristine (0 s) and Ti-treated (2 s) hematite photoanodes. The IPCE data were measured at 1.23 V *vs* RHE.

be amorphous TiO_2 according to the property of a $TiCl_4$ solution exposed to humid air. It is also clear that the thickness of the coating layer increases with the treatment time. In the Supporting Information S3 we show the SEM and HRTEM images of the hematite samples treated for 5 and 10 s, and the results strongly support the temporal thickness evolution. By this facile method we can control the shortest treating time of 2 s to obtain a 2 nm thick layer. Elemental mapping and an energy dispersive X-ray analysis (EDX) spectrum of Ti-treated hematite (2 s) are also shown in the Supporting Information S4, where the results clearly reveal the existence of Ti in the sample.

X-ray diffraction (XRD) data of the pristine and Ti-treated hematite nanostructures are shown in the Supporting Information S5. Data confirmed the existence of a typical hematite structure (JCPDS 33-0664). No additional peak or peak shift can be observed, although there is an obvious coating layer on hematite for Ti-treated samples. It can be attributed to the amorphous structure of the coating layer in agreement with HRTEM results.[21]

The photocurrent density-applied potential (*J*−*V*) scans of the pristine and Ti-treated hematite photoanodes are shown in Figure 2a. It is clear that Ti treatment exhibits an obvious positive effect on the performance of the hematite photoanodes. Especially, the Ti-treated hematite with a treating time of 2 s shows a significant improvement of the photocurrent from 0.64 mA/cm^2 (pristine hematite) to 1.44 mA/cm^2 at 1.23 V *vs* RHE. As the treatment time increases, the photocurrent decreases with increasing thickness of the coating layer. When the treatment time is 20 s, the photocurrent shows a very low value of 0.48 mA/cm^2 at 1.23 V *vs* RHE, which is even lower than that of the pristine sample. The onset potential of the Ti-treated hematite with the treatment time of 20 s also increases greatly. The results show that a thin surface coating (such as 2 nm) enhances the performance of hematite, but a thicker coating leads to a worse performance. Unfortunately, by the present Ti treatment method it is limited to the shortest treating time of about 2 s (corresponding to 2 nm in thickness), although a thinner layer may possibly produce a better performance.

The incident photon-to-current conversion efficiency (IPCE) data of the pristine and Ti-treated (2 s) hematite photoanodes are shown in Figure 2b (at 1.23 V *vs* RHE). The IPCE of the Ti-treated sample shows an obvious enhancement compared to that of the pristine hematite, which is consistent with the *J*−*V* curves. The IPCE enhancement of the Ti-treated sample can be observed in the whole detected range. Since the IPCE data of TiO_2 are typically around zero at a wavelength above 380 nm, the result suggests that the enhanced photocurrent is not due to the photoresponse of TiO_2.[15] The stability tests of the pristine and Ti-treated (2 s) hematite photoanodes are also shown in the Supporting Information S6. The photocurrent of the Ti-treated (2 s) hematite photoanode keeps a stable value after 2 h. The totality of the results shows that simple evaporation of a $TiCl_4$ solution on the surface of FeOOH is an effective way to prepare Ti-treated hematite for efficient solar water oxidation.

To prepare Ti-treated hematite with thinner coating layer (less than 2 nm) for high performance, we developed a HF-assisted Ti treatment method. The detailed description of the treatment is shown in the Experimental Section, and the experimental setup is shown in the Supporting Information S2. HF solution is mainly used for the dissolution of Ti, which will adsorb on the surface of FeOOH to form a Ti-based layer after annealing. The SEM image of HF-Ti-treated (30 s) hematite nanostructures (shown in the Supporting Information S7) is similar to that of the pristine hematite. An HRTEM image and elemental mapping of the HF-Ti-treated hematite (30 s) are also shown in Figure 3. No obvious coating can be observed, but the elemental mapping clearly reveals the existence of Ti, suggesting it is an ultrathin layer. X-ray photoelectron spectroscopy (XPS) data in the Supporting Information S8 also clearly confirm the existence of Ti. XRD data of the

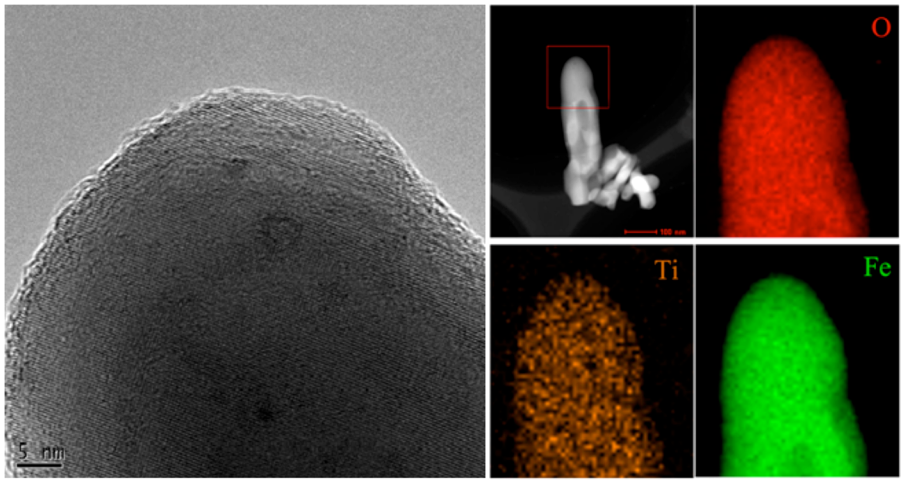

Figure 3. (Left) HRTEM image of HF-Ti-treated (30 s) hematite nanostructures. (Right) Dark-field image of TEM and the corresponding TEM elemental mappings of HF-Ti-treated (30 s) hematite nanostructures (rectangle box marked area): O (red), Ti (yellow), and Fe (green) distribution in the selected area.

HF-Ti-treated hematite nanostructures (Supporting Information S9) show the hematite structure. Thus, the HF-Ti-treated sample can be assigned as hematite nanostructures with an ultrathin Ti-based layer.

The performances of HF-Ti-treated hematite photoanodes are shown in Figure 4. In Figure 4a the HF-Ti-treated samples exhibit significantly improved photocurrent. Especially, HF-Ti-treated hematite with a treatment time of 30 s shows a good photocurrent of 2.0 mA/cm^2 at 1.23 V *vs* RHE, which is more than 3 times that of the pristine hematite (also much higher than the performance of the $TiCl_4$-treated sample). Moreover, the performance of the HF-Ti-treated (30 s) hematite photoanode can be further improved by coupling Co-Pi catalysts, which achieves a high photocurrent of 2.6 mA/cm^2 at 1.23 V *vs* RHE and a max photocurrent of 3.62 mA/cm^2 at 1.6 V *vs* RHE. The results are comparable to the high performance of hematite reported recently.[4,19−21] In recent years the benchmark performance was achieved by the cauliflower-type hematite nanostructure prepared by the APCVD method with an IrO_2 catalyst, which showed a photocurrent of 3.3 mA/cm^2 at 1.23 V *vs* RHE and a plateau photocurrent of 3.75 mA/cm^2.[5] However, the performance was instable using an IrO_2 catalyst.[4,5] Co-Pi catalysts were also used on the APCVD-grown hematite to get a stable performance with a photocurrent of 2.8 mA/cm^2 at 1.23 V *vs* RHE.[4] Recently the colloidal nanocrystal deposition process coupled with Sn-doping was used to prepare highly efficient hematite photoanodes with an excellent photocurrent of 2.7 mA/cm^2 at 1.23 V *vs* RHE.[19] A 3D nanophotonic structure was also developed as the substrate of ultrathin films of hematite to largely improve the light absorption, which showed a high photocurrent of 3.05 mA/cm^2 at 1.23 V *vs* RHE.[21] Compared to the APCVD method, the colloidal nanocrystal deposition process, or a 3D nanophotonic structure, our simple

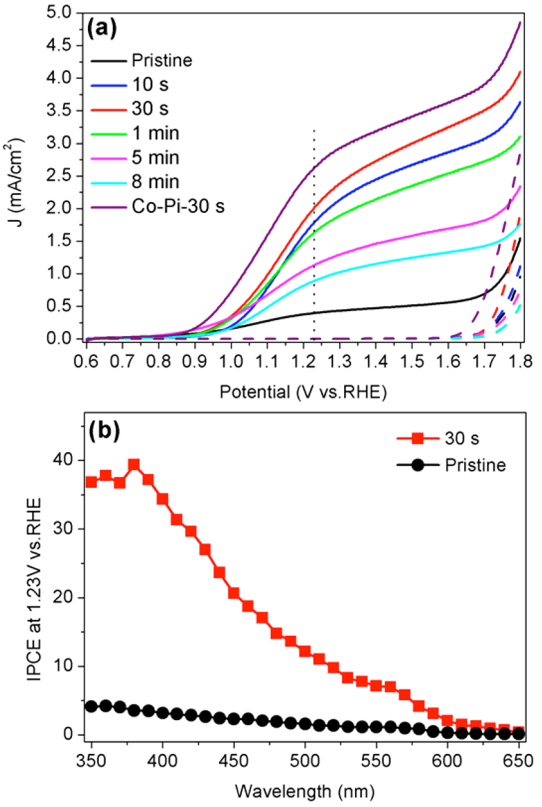

Figure 4. (a) *J*−*V* curves of the pristine hematite photoanode, HF-Ti-treated hematite photoanodes with different treatment times (10 s, 30 s, 1 min, 5 min, and 8 min), and a Co-Pi-decorated HF-Ti-treated (30 s) hematite photoanode (Co-Pi-30 s). (b) IPCE spectra of the pristine and HF-Ti-treated (30 s) hematite photoanodes. The IPCE data were measured at 1.23 V *vs* RHE.

hydrothermal method and facile Ti treatment by immersing the FeOOH in Ti-dissolved HF solution show great advantages in preparing efficient hematite photoanodes with comparable performance. The IPCE data of HF-Ti-treated (30 s) hematite photoanodes are shown in Figure 4b (at 1.23 V *vs* RHE), exhibiting an

obvious enhancement compared to that of the pristine hematite, in agreement with the $J-V$ curves.

To reveal the mechanism for enhanced performance by Ti treatment, Mott−Schottky plots of the pristine and Ti-treated ($TiCl_4$-treated, 2 s) hematite photoanodes are shown in the Supporting Information S10. The slopes are used to estimate carrier densities.[22,23] For the pristine hematite, the carrier density is calculated to be 3.55×10^{20} cm^{-3}, while the value is 4.76×10^{20} cm^{-3} for Ti-treated (2 s) hematite. There is no big difference between the samples before and after Ti treatment, indicating that the significantly improved photocurrent after Ti treatment is not mainly from increased conductivity.[13,15]

XPS and XAS experiments were performed to explore the electronic structure and chemical state of hematite nanostructures before and after Ti treatment. In the Supporting Information S11 we show the XPS survey scan of pristine and Ti-treated (2 s) hematite. It is clear that after the Ti treatment there is an obvious Ti signal in the sample. The Ti 2p XPS spectrum of Ti-treated hematite shows a similar energy position to that of TiO_2, indicating Ti in Ti-treated hematite has an oxidation state of Ti^{4+}.[17,24]

Further characterization of the compositions in Ti-treated hematite by XAS is shown in Figure 5. Figure 5a and b show the O K-edge and Ti L-edge XAS spectra of the pristine and Ti-treated samples, respectively. XAS stands for the excitation of electrons from a core level to local and partial empty states, which is an effective tool to probe the electronic states of complex materials.[12] In Figure 5a the O K-edge spectrum of the pristine sample exhibits three separated prepeaks (A1−A3) and two main peaks (B1 and B2). The prepeaks A1 and A2 can be attributed to typical hematite features related to transitions to antibonding O 2p states hybridized with Fe 3d states.[25,26] The main peaks B1 and B2 can be assigned to oxygen 2p states hybridized with Fe 4s and 4p states.[25] An additional peak A3 is also observed, which might be attributed to carbon contaminations.[27] The spectrum of the Ti-treated hematite shows similar features to those of pristine hematite. However, the peak intensities are different from those of pristine hematite due to the Ti-based coating layer. To clarify the electronic structure of the coating layer, we show in Figure 5a the magnified difference spectrum (Ti-treated hematite subtracting pristine hematite, with the spectrum of Ti-treated hematite normalized to make sure the difference spectrum has no negative value) and compare it with some reference spectra. It is clear that the difference spectrum shows a similar spectral shape to that of rutile and anatase TiO_2 with two prepeaks (C1 and C2) and four peaks labeled D1−D4 at higher energies.[28,29] Although the difference spectrum looks similar to that of rutile and anatase TiO_2, it is not the same as any of them. It has a stronger D3 than D4, which is similar to

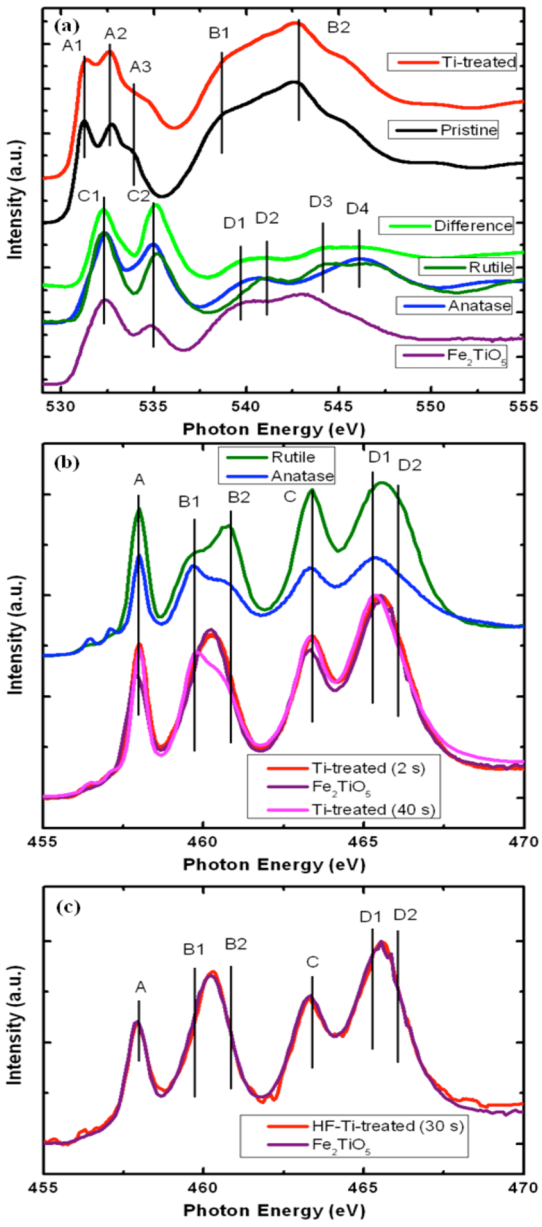

Figure 5. (a) O K-edge XAS spectra of the pristine and Ti-treated (2 s) hematite nanostructures compared with the spectra of rutile TiO_2, anatase TiO_2, and Fe_2TiO_5. The difference spectrum between the pristine and Ti-treated hematite is also shown. (b) Ti L-edge XAS spectra of Ti-treated (2 and 40 s) hematite nanostructures compared with the spectra of rutile TiO_2, anatase TiO_2, and Fe_2TiO_5. (c) Ti L-edge XAS spectrum of HF-Ti-treated (30 s) hematite nanostructures compared with the spectrum of Fe_2TiO_5.

that of rutile TiO_2, while the intense peak D1 shows a similar shape to that of anatase TiO_2. The intense D1 peak could also be from Fe_2TiO_5 (shown as a reference spectrum). However, because of the strong influence from underneath hematite at the O K-edge, it is hard to identify the composition of the Ti-based coating layer only by the difference spectrum.

The Ti L-edge XAS signal comes only from the coating layer of the sample and can be used to exactly identify the composition. The Ti L-edge spectra of

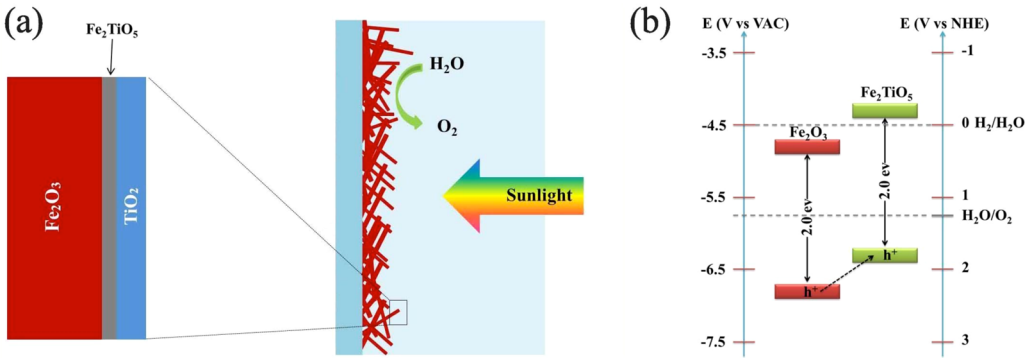

Figure 6. (a) Illustration of the compositions in Ti-treated hematite. (b) Band structure of Fe_2TiO_5 and hematite.

Ti-treated hematite and some reference samples are shown in Figure 5b. The reference spectra of rutile and anatase TiO_2 show clear main peaks A–D. The assignment of the peaks can be found in the literature.[28,29] Briefly, peaks A and B (B1 and B2) can be attributed to Ti L_3-edge features, while peaks C and D (D1 and D2) can be attributed to Ti L_2-edge features.[28,29] For both Ti L_2 and L_3 edges, the crystal field splitting of the 3d band will produce t_{2g} (peaks A and C) and e_g (peaks B and D) subbands.[28,29] It is also worthy to know that for both rutile and anatase TiO_2 the e_g-related peaks (B and D) will further split into two peaks, as shown in Figure 5b, labeled B1, B2, D1, and D2.[28,29] The splitting of peak D into D1 and D2 is not well resolved because of the lifetime-related broadening of the L_2 edge.[28] The Ti-treated (2 s) hematite sample shows a similar spectral shape to that of rutile or anatase TiO_2. However, the doublet peaks B1 and B2 disappear in the Ti-treated (2 s) sample, while a single peak located at the center between B1 and B2 can be observed, suggesting that the Ti-based coating layer (2 s) on hematite is neither rutile nor anatase TiO_2. Interestingly, the spectrum of the Ti-treated (2 s) hematite is almost identical to that of Fe_2TiO_5 (with only peak A having different intensity); especially a single peak B appears at the center between peaks B1 and B2. The resemblance of the two spectra suggests the coating to be an Fe_2TiO_5 structure. The results are in good agreement with the literature for similar compounds such as Al_2TiO_5.[30] In recent reports, amorphous TiO_2 was also suggested to be the effective component for solar water oxidation in Ti-treated hematite.[12,15] Although amorphous TiO_2 also has a single peak B without the doublet structure of B1 and B2 according to previous XAS results, the energy position of peak B for amorphous TiO_2 is at a lower position near peak B1,[28,29] which is significantly different from our result (2 s) with a peak B located at the center between peaks B1 and B2. The data strongly suggest that a coating layer of Fe_2TiO_5 structure on hematite was produced.

In the Ti-treated process by $TiCl_4$, TiO_2 can be formed on FeOOH during the exposure process. However, a further annealing process at a temperature higher than 500 °C might introduce Fe_2TiO_5 structure when TiO_2 is reacted with hematite. The surface layer of Fe_2TiO_5 will form a heterojunction structure with hematite due to favorable band structure.[31] The illustration of the compositions in Ti-treated hematite is shown in Figure 6a. The band structures of Fe_2TiO_5 and hematite are also shown in Figure 6b. The UV–vis spectrum in the Supporting Information S12 has been used to estimate the band gap of our Fe_2TiO_5 sample, which is about 2.0 eV. Ultraviolet photoelectron spectroscopy (UPS) in the Supporting Information S13 is used to measure the top of the valence band (VB, about −6.31 eV compared to the vacuum level). Thus, the band structure of our Fe_2TiO_5 sample can be obtained in Figure 6b (0 V *vs* RHE equals −4.5 V *vs* VAC), which is in good agreement with the literature.[31] It is clear that the top of the VB of Fe_2TiO_5 is slightly higher than that of hematite, which would favor the hole transportation from hematite to Fe_2TiO_5 and reduce photoexcited hole accumulation on the surface of hematite. The performance can thus be improved by the heterostructure of Fe_2TiO_5 and hematite.[31] A similar effect was also reported for the Fe_2TiO_5–TiO_2 heterostructure, which improved the performance of TiO_2 for solar water oxidation.[31]

The formation of the Fe_2TiO_5-hematite heterostructure can also explain the thickness effect of the coating layer. As the treatment time increases, a thicker coating layer would be produced on hematite, but the increased part could not react with hematite to produce further formation of Fe_2TiO_5. Formation of the top layer of TiO_2 would not help the water oxidation process; instead it might reduce photoabsorption, leading to decreased performance, as shown in Figure 2a. We also show in Figure 5b the Ti L-edge XAS spectrum of a Ti-treated hematite sample after a longer treating time of 40 s. A different peak B with doublet peaks B1 and B2 (B1 is higher than B2, standing for the anatase TiO_2) can be observed, indicating that the top layer after long exposure time of $TiCl_4$ is TiO_2. Our HRTEM image in the Supporting Information S14 also confirms the anatase TiO_2 structure.

The Ti L-edge spectrum of HF-Ti-treated (30 s) hematite with an ultrathin Ti-based layer is also shown in Figure 5c compared with the spectrum of Fe_2TiO_5. Similar to $TiCl_4$-treated hematite, HF-Ti-treated (30 s) hematite also shows a single peak B located at the center position between peaks B1 and B2, indicating the formation of Fe_2TiO_5. Interestingly, the spectrum of HF-Ti-treated (30 s) hematite is almost identical to that of the reference Fe_2TiO_5. Note that the spectra of $TiCl_4$-treated hematite and Fe_2TiO_5 show a slight difference in the intensity of peak A, which can be attributed to the existence of TiO_2 in the top layer. However, the spectra of the HF-Ti-treated (30 s) sample and Fe_2TiO_5 are almost completely identical due to the ultrathin layer. When the FeOOH sample on an FTO substrate was immersed in the Ti-dissolved HF solution, Ti ions adsorbed on the surface of FeOOH, and the etching of FeOOH by HF may favor this process. The following annealing process in air will produce amorphous TiO_2, which can react with hematite to form an ultrathin layer of Fe_2TiO_5. Thus, the Fe_2TiO_5-hematite heterostructure can be formed to yield a good performance. The Fe L-edge spectrum of HF-Ti-treated (30 s) hematite is also shown in the Supporting Information S15 compared with the spectra of pristine and HF-treated hematite samples. The spectrum of the Fe_2TiO_5 reference is also shown. There is almost no difference between the samples before and after HF-assisted Ti treatment within the experimental error, which can be attributed to the main contribution from the underneath hematite (the spectrum of pure Fe_2TiO_5 is also similar to that of hematite). The effect of HF solution has also been investigated, and the $J-V$ scans of HF-treated (without Ti dissolution) hematite photoanodes are shown in the Supporting Information S16. HF treatment also improves the photocurrent of hematite, as shown in the $J-V$ curves, which might be attributed to a surface etching effect similar to the HCl-treated hematite.[10] However, the best performance of hematite after HF treatment is only 1.2 mA/cm^2 at 1.23 V *vs* RHE, which is far below that after HF-Ti treatment, and thus the high performance of the HF-Ti-treated sample should be mainly attributed to the formation of an Fe_2TiO_5-hematite heterostructure. The XPS results of HF-treated hematite (shown in the Supporting Information S17) show no F signal after annealing, suggesting that the improved performance is not an effect of F-doping. Pure Fe_2TiO_5 (without hematite) was also reported for solar water oxidation, but its performance was low (less than 0.5 mA/cm^2 at 1.23 V *vs* RHE).[32] Our results reveal that the formation of the Fe_2TiO_5-hematite heterostructure is effectively responsible for enhancing solar water oxidation.

The Fe_2TiO_5-hematite heterostructure can also be applied to understand the enhanced performance of other Ti-treated hematite nanostructures. For example, Yang *et al*. recently reported that an ultrathin TiO_2 layer ALD-grown on hematite led to increased photocurrent and cathodic shift of the onset potential,[15] whereas Sivula *et al*. revealed that ALD-grown TiO_2 had no positive effect on the performance of hematite.[8] Their differences may be attributed to different conditions of postgrowth annealing (no higher than 400 °C for Sivula *et al*. and 400−600 °C for Yang *et al*.).[15] Our results suggest a reasonable explanation that the Fe_2TiO_5-hematite heterostructure introduced by annealing would improve the performance by reducing photoexcited hole accumulation. Further, the reported thickness dependence of the performance was also in good agreement with our results.[15] The Fe_2TiO_5-hematite heterostructure can be applied to understand the beneficial effects of other Ti-treated processes such as "Ti-doping" in hematite. A recent work studied the XAS data for various Ti incorporation in hematite and their electronic structure for enhanced performance.[12] Comparing the Ti L-edge XAS data for various Ti-treated hematites,[12] we find many of them show a similar Fe_2TiO_5 structure to ours with a single peak B located at the center between peaks B1 and B1. We thus hypothesize that some of the Ti-treated (or doped) hematite was actually Fe_2TiO_5 in hematite, instead of the typically accepted doping with Ti substitution of Fe in hematite. Actually, the XAS data showed no evidence for the existence of Fe^{2+} for $FeTiO_3$ after various Ti treatments.[12] Although "Ti-doping" was widely accepted for Ti-treated hematites and XPS data revealed the existence of Ti,[13,17] those results nevertheless do not provide direct evidence for Ti substitution of Fe in hematite. On the other hand, the totality of our results offers a convincing mechanism for the enhanced performance of Ti-treated hematite due to the formation of the Fe_2TiO_5-hematite heterostructure. Our results may provide a new perspective to understand the enhanced performance of Ti treatment processes in hematite.

CONCLUSIONS

We prepared an Fe_2TiO_5-hematite heterostructure for efficient solar water oxidation. The photocurrent of a hematite photoanode with an ultrathin Fe_2TiO_5 layer shows significant improvement (2.0 mA/cm^2 at 1.23 V *vs* RHE) compared to that of a pristine hematite photoanode. It can be further improved by coupling with Co-Pi catalysts to achieve a high value of 2.6 mA/cm^2 at 1.23 V *vs* RHE. Synchrotron-based soft X-ray absorption spectroscopy analyses clearly revealed the existence of Fe_2TiO_5 structure on hematite forming a heterojunction, which reduced the photogenerated hole accumulation and thus improved the performance. Our results suggest that the Fe_2TiO_5-hematite heterostructure is a very effective component for solar water oxidation. Moreover,

the new Fe_2TiO_5-hematite heterostructure may provide an insight into understanding the enhanced performance of other Ti-treated hematite nanostructures.

EXPERIMENTAL SECTION

Photoanode Preparation. A modified hydrothermal method was used to prepare the pristine hematite photoanodes grown on a fluorine-doped SnO_2 (Nippon Sheet Glass, Japan, 14 ohm/sq) glass substrate.[11] Briefly, 1 M sodium nitrate ($NaNO_3$, Sinopharm Chemical Reagent Co., Ltd.) and 50 μL of HCl (45.3−45.8 wt %) were added into a 50 mL aqueous solution of 0.15 M ferric chloride ($FeCl_3 \cdot 6H_2O$, Sinopharm Chemical Reagent Co., Ltd.) for the hydrothermal reaction, into which a washed FTO glass (40 mm × 30 mm × 2 mm) was placed.[16] The reaction autoclave was heated to 95 °C for 4 h. A uniform film of iron oxyhydroxides (FeOOH) was then formed on the FTO substrate. The samples were further sintered in air at 550 °C for 2 h and at 750 °C for an additional 10 min. The final product was labeled as the pristine hematite.

To prepare Ti-treated hematite by evaporating $TiCl_4$ (labeled as Ti-treated hematite), 10 μL of titanium tetrachloride ($TiCl_4$, Sinopharm Chemical Reagent Co., Ltd.) was placed on the bottom of a watch glass, which was quickly covered by the FeOOH sample on the FTO substrate (cut to 20 mm × 30 mm × 2 mm) for a covering time from 2 to 20 s. $TiCl_4$ is a highly volatile metal halide, which forms an opaque cloud of titanium dioxide (TiO_2) and hydrogen chloride (HCl) when exposed to humid air. After covering the $TiCl_4$, a thin layer of TiO_2 is deposited on the FeOOH. The sample was then sintered in air at 550 °C for 2 h and at 750 °C for an additional 10 min to get Ti-treated hematite. The experimental setup is shown in the Supporting Information S1.

For the HF-assisted Ti treatment, 50 mg of Ti foil (thickness of 25 μm) was thoroughly dissolved in a hydrofluoric acid (HF) aqueous solution (1 mL of HF solution (48 wt %) mixed with 49 mL of deionized water). The FeOOH sample on the FTO substrate (cut to 25 mm × 30 mm × 2 mm) was put into the solution for various treatment times from 10 s to 8 min. The sample was then sintered in air at 550 °C for 2 h and at 750 °C for an additional 10 min to get the final product (labeled as HF-Ti-treated hematite). The experimental setup is shown in the Supporting Information S2. The final HF-Ti-treated (30 s) hematite sample was also decorated with cobalt phosphate to further improve the performance by photoassisted electrodeposition in a three-electrode system (see ref 4).

Structural Characterization. A scanning electron microscope (FEI Quanta 200F) was used for the SEM images. UV−vis spectra were recorded on a Lambda 750 spectrophotometer. We used an X-ray photoelectron spectrometer (XPS, Kratos AXIS UltraDLD) and X-ray diffraction (XRD, PANalytical, Zmpyrean) for the structure characterization. UPS spectra were measured with a He I (21.22 eV) gas discharge lamp (a bias of 4 V has been applied). X-ray absorption spectra were collected at the Beijing Synchrotron Radiation Facility (BSRF), the Shanghai Synchrotron Radiation Facility (SSRF, 08U), and the Synchrotron Radiation Research Center (SRRC) in Hsinchu (Taiwan). TEM images were obtained with a FEI/Philips Techai 12 Bio-TWIN transmission electron microscope, while HRTEM images and EDX spectroscopy were obtained with a CM200 FEG transmission electron microscope.

Photoelectrochemical Experimentals. The working area of hematite photoanodes was about 0.1 cm^2 with the left part covered by nonconductive hysol epoxy. An electrochemical workstation (CHI 660D) was used for the PEC measurements. A Pt wire was used as a counter electrode, and an Ag/AgCl electrode was used as a reference. The pH value of the electrolyte (1 M NaOH) was about 13.6. The measured voltage was converted into the potential *vs* RHE. The scan rate of the potential was 50 mV s^{-1} from 0.6 to 1.8 V *vs* RHE. The light source was a xenon high brightness cold light source (XD-300) equipped with an AM 1.5 filter, and the light power density was 100 mW/cm^2. A xenon lamp (CEL-HXF300/CEL-HXBF300, 300W) coupled with a monochromator (Omni-λ3005) was used to measure the IPCE data. The bias voltage for the Mott−Schottky plots was scanned from −0.4 to 0.1 V *vs* Ag/AgCl in the dark at a frequency of 1 kHz.

Conflict of Interest: The authors declare no competing financial interest.

Acknowledgment. We acknowledge the support from BSRF, SSRF, and SRRC for the XAS experiments. This work is supported by the National Basic Research Development Program of China (2012CB825800), the National Natural Science Foundation of China (U1432249, 11275137, 11179032), the Priority Academic Program Development of Jiangsu Higher Education Institutions (PAPD), and Innovative Research Teams of Jiangsu Higher Education Institutions.

Supporting Information Available: Experimental setup, SEM and TEM images, XRD data, photochemical stability curves, Mott−Schottky plots, *J*−*V* scans of the pristine and HF-treated (without Ti dissolution) hematite photoanodes, UV−vis spectrum, and UPS and XPS results. This material is available free of charge *via* the Internet at http://pubs.acs.org.

REFERENCES AND NOTES

1. Sivula, K.; Le Formal, F.; Grätzel, M. Solar Water Splitting: Progress Using Hematite (α-Fe_2O_3) Photoelectrodes. *ChemSusChem* **2011**, *4*, 432–449.
2. Lin, Y. J.; Yuan, G. B.; Stafford, S.; Zhou, S.; Wang, D. W. Hematite-Based Solar Water Splitting: Challenges and Opportunities. *Energy Environ. Sci.* **2011**, *4*, 4862–4869.
3. Murphy, A. B.; Barnes, P. R. F.; Randeniya, L. K.; Plumb, I. C.; Grey, I. E.; Horne, M. D.; Glasscock, J. A. Efficiency of Solar Water Splitting Using Semiconductor Electrodes. *Int. J. Hydrogen Energy* **2006**, *31*, 1999–2017.
4. Zhong, D. K.; Cornuz, M.; Sivula, K.; Grätzel, M.; Gamelin, D. R. Photo-Assisted Electrodeposition of Cobalt−Phosphate (Co−Pi) Catalyst on Hematite Photoanodes for Solar Water Oxidation. *Energy Environ. Sci.* **2011**, *4*, 1759–1764.
5. Tilley, S. D.; Cornuz, M.; Sivula, K.; Grätzel, M. Light-Induced Water Splitting with Hematite: Improved Nanostructure and Iridium Oxide Catalysis. *Angew. Chem., Int. Ed.* **2010**, *49*, 6405–6408.
6. Franking, R.; Li, L. S.; Lukowski, M. A.; Meng, F.; Tan, Y.; Hamers, R. J.; Jin, S. Facile Post-Growth Doping of Nanostructured Hematite Photoanodes for Enhanced Photoelectrochemical Water Oxidation. *Energy Environ. Sci.* **2013**, *6*, 500–512.
7. Du, C.; Yang, X. G.; Mayer, M. T.; Hoyt, H.; Xie, J.; McMahon, G.; Bischoping, G.; Wang, D. W. Hematite-Based Water Splitting with Low Turn-On Voltages. *Angew. Chem., Int. Ed.* **2013**, *52*, 12692–12695.
8. Le Formal, F.; Tétreault, N.; Cornuz, M.; Moehl, T.; Grätzel, M.; Sivula, K. Passivating Surface States on Water Splitting Hematite Photoanodes with Alumina Overlayers. *Chem. Sci.* **2011**, *2*, 737–743.
9. Liu, R.; Zheng, Z.; Spurgeon, J.; Yang, X. G. Enhanced Photoelectrochemical Water-Splitting Performance of Semiconductors by Surface Passivation Layers. *Energy Environ. Sci.* **2014**, *7*, 2504–2517.
10. Cao, D. P.; Luo, W. J.; Feng, J. Y.; Zhao, X.; Li, Z. S.; Zou, Z. G. Cathodic Shift of Onset Potential for Water Oxidation on a Ti^{4+} Doped Fe_2O_3 Photoanode by Suppressing the Back Reaction. *Energy Environ. Sci.* **2014**, *7*, 752–759.
11. Ling, Y. C.; Wang, G. M.; Wheeler, D. A.; Zhang, J. Z.; Li, Y. Sn-Doped Hematite Nanostructures for Photoelectrochemical Water Splitting. *Nano Lett.* **2011**, *11*, 2119–2125.
12. Kronawitter, C. X.; Zegkinoglou, I.; Shen, S. H.; Liao, P.; Cho, I. S.; Zandi, O.; Liu, Y. S.; Lashgari, K.; Westin, G.; Guo, J. H.; *et al.*

Titanium Incorporation into Hematite Photoelectrodes: Theoretical Considerations and Experimental Observations. *Energy Environ. Sci.* **2014**, *7*, 3100–3121.
13. Zandi, O.; Klahr, B. M.; Hamann, T. W. Highly Photoactive Ti-Doped α-Fe_2O_3 Thin Film Electrodes: Resurrection of the Dead Layer. *Energy Environ. Sci.* **2013**, *6*, 634–642.
14. Kronawitter, C. X.; Bakke, J. R.; Wheeler, D. A.; Wang, W. C.; Chang, C. L.; Antoun, B. R.; Zhang, J. Z.; Guo, J. H.; Bent, S. F.; Mao, S. S.; *et al*. Electron Enrichment in 3d Transition Metal Oxide Hetero-Nanostructures. *Nano Lett.* **2011**, *11*, 3855–3861.
15. Yang, X. G.; Liu, R.; Du, C.; Dai, P. C.; Zheng, Z.; Wang, D. W. Improving Hematite-Based Photoelectrochemical Water Splitting with Ultrathin TiO_2 by Atomic Layer Deposition. *ACS Appl. Mater. Interfaces* **2014**, *6*, 12005–12011.
16. Deng, J. J.; Zhong, J.; Pu, A. W.; Zhang, D.; Li, M.; Sun, X. H.; Lee, S. T. Ti-Doped Hematite Nanostructures for Solar Water Splitting with High Efficiency. *J. Appl. Phys.* **2012**, *111*, 084312–7.
17. Wang, G. M.; Ling, Y. C.; Wheeler, D. A.; George, K. E.; Horsley, K.; Heske, C.; Zhang, J. Z.; Li, Y. Facile Synthesis of Highly Photoactive α-Fe_2O_3-Based Films for Water Oxidation. *Nano Lett.* **2011**, *11*, 3503–3509.
18. Cho, I. S.; Lee, C. H.; Feng, Y.; Logar, M.; Rao, P. M.; Cai, L.; Kim, D. R.; Sinclair, R.; Zheng, X. L. Codoping Titanium Dioxide Nanowires with Tungsten and Carbon for Enhanced Photoelectrochemical Performance. *Nat. Commun.* **2013**, *4*, 1723–1730.
19. Goncalves, R. H.; Leite, E. R. The Colloidal Nanocrystal Deposition Process: An Advanced Method to Prepare High Performance Hematite Photoanodes for Water Splitting. *Energy Environ. Sci.* **2014**, *7*, 2250–2254.
20. Qiu, Y.; Leung, S. F.; Zhang, Q.; Hua, B.; Lin, Q.; Wei, Z.; Tsui, K. H.; Zhang, Y.; Yang, S. H.; Fan, Z. Y. Efficient Photoelectrochemical Water Splitting with Ultrathin Films of Hematite on Three-Dimensional Nanophotonic Structures. *Nano Lett.* **2014**, *14*, 2123–2129.
21. Xi, L. F.; Chiam, S. Y.; Mak, W. F.; Tran, P. D.; Barber, J.; Loo, S. C. J.; Wong, L. H. A Novel Strategy for Surface Treatment on Hematite Photoanode for Efficient Water Oxidation. *Chem. Sci.* **2013**, *4*, 164–169.
22. Deng, J. J.; Lv, X. X.; Gao, J.; Pu, A. W.; Li, M.; Sun, X. H.; Zhong, J. Facile Synthesis of Carbon-Coated Hematite Nanostructures for Solar Water Splitting. *Energy Environ. Sci.* **2013**, *6*, 1965–1970.
23. Li, M.; Deng, J. J.; Pu, A. W.; Zhang, P. P.; Zhang, H.; Gao, J.; Hao, Y. Y.; Zhong, J.; Sun, X. H. Hydrogen-Treated Hematite Nanostructures with Low Onset Potential for Highly Efficient Solar Water Oxidation. *J. Mater. Chem. A* **2014**, *2*, 6727–6733.
24. Briggs, D.; Seah, M. P. *Auger and X-Ray Photoelectron Spectroscopy: Practical Surface Analysis*; Wiley: New York, 1990; Vol. 1, Appendix 1.
25. Wu, Z. Y.; Gota, S.; Jollet, F.; Polllak, M.; Soyer, M. G.; Natoli, C. R. Characterization of Iron Oxides by X-ray Absorption at the Oxygen K Edge Using a Full Multiple-Scattering Approach. *Phys. Rev. B* **1997**, *55*, 2570–2577.
26. Braun, A.; Sivula, K.; Bora, D. K.; Zhu, J. F.; Zhang, L.; Grätzel, M.; Guo, J. H.; Constable, E. C. Direct Observation of Two Electron Holes in a Hematite Photoanode during Photoelectrochemical Water Splitting. *J. Phys. Chem. C* **2012**, *116*, 16870–16875.
27. Braun, A.; Bayraktar, D.; Erat, S.; Harvey, A. S.; Beckel, D.; Purton, J. A.; Holtappels, P.; Gauckler, L. J.; Graule, T. Pre-edges in Oxygen (1s) X-ray Absorption Spectra: A Spectral Indicator for Electron Hole Depletion and Transport Blocking in Iron Perovskites. *Appl. Phys. Lett.* **2009**, *94*, 202102–4.
28. Kucheyev, S. O.; van Buuren, T.; Baumann, T. F.; Satcher, J. H., Jr.; Willey, T. M.; Meulenberg, R. W.; Felter, T. E.; Poco, J. F.; Gammon, S. A.; Terminello, L. J. Electronic Structure of Titania Aerogels from Soft X-ray Absorption Spectroscopy. *Phys. Rev. B* **2004**, *69*, 245102–7.
29. Kronawitter, C. X.; Kapilashrami, M.; Bakke, J. R.; Bent, S. F.; Chuang, C. H.; Pong, W. F.; Guo, J. H.; Vayssieres, L.; Mao, S. S. TiO_2-SnO_2:F Interfacial Electronic Structure Investigated by Soft X-ray Absorption Spectroscopy. *Phys. Rev. B* **2012**, *85*, 125109–7.
30. Soriano, L.; Abbate, M.; Fernández, A.; González-Elipe, A. R.; Sanz, J. M. Chemical Analysis of Ternary Ti Oxides Using Soft X-ray Absorption Spectroscopy. *Surf. Interface Anal.* **1997**, *25*, 804–808.
31. Courtin, E.; Baldinozzi, G.; Sougrati, M. T.; Stievano, L.; Sanchez, C.; Laberty-Robert, C. New Fe_2TiO_5-Based Nanoheterostructured Mesoporous Photoanodes with Improved Visible Light Photoresponses. *J. Mater. Chem. A* **2014**, *2*, 6567–6577.
32. Bassi, P. S.; Chiam, S. Y.; James Barber, G.; Wong, L. H. Hydrothermal Grown Nanoporous Iron Based Titanate, Fe_2TiO_5 for Light Driven Water Splitting. *ACS Appl. Mater. Interfaces* **2014**, *6*, 22490–22495.